Bulletin of the Seismological Society of America, Vol. XX, No. XX, pp. –, – 2019, doi: 10.1785/0120190057

Ⓔ

Tracking Induced Seismicity in the Fort Worth Basin: A Summary of the 2008–2018 North Texas Earthquake Study Catalog

by Louis Quinones, Heather R. DeShon, SeongJu Jeong, Paul Ogwari, Oner Sufri, Monique M. Holt, and Kevin B. Kwong

Abstract Since 2008, earthquake sequences within the Fort Worth basin (FWB), north Texas, have been linked to wastewater disposal activities related to unconventional shale-gas production. The North Texas Earthquake Study (NTXES) catalog (2008–2018), described and included herein, uses a combination of local and regional seismic networks to track significant seismic sequences in the basin. The FWB earthquakes occur along discrete faults that are relatively far apart (>30 km), allowing for more detailed study of individual sequence development. The three largest sequences (magnitude 3.6+) are monitored by local seismic networks (<15 km epicentral distances), whereas basinwide seismicity outside these three sequences is monitored using regional distance stations. A regional 1D velocity model for the FWB reflects basinwide well log, receiver function, and regional crustal structure studies and is modified for the larger individual earthquake sequences using local well-log and geology data. Here, we present an m_{b_Lg} relationship appropriate for Texas and a basin-specific M_L relationship, both calculated using attenuation curves developed with the NTXES catalog. Analysis of the catalog reveals that the earthquakes generally occur within the Precambrian basement formation along steeply dipping normal faults, and although overall seismicity rates have decreased since 2016, new faults have become active. Between 2006 and 2018, more than 2 billion barrels of fluids were injected into the Ellenburger formation within the FWB. We observe strong spatial and temporal correlations between the earthquake locations and wastewater disposal well locations and injection volumes, implying that fluid injection activities may be the main driving force of seismicity in the basin. In addition, we observe seismicity occurring at greater distances from injection wells (>10 km) over time, implying that far-field stress changes associated with fluid injection activities may be an important component to understanding the seismic hazard of induced seismicity sequences.

Supplemental Content: Velocity models used to locate the North Texas Earthquake Study (NTXES) catalog earthquakes, magnitude differences across catalogs of seismicity in the Fort Worth basin (FWB), the strike distribution of the 68% confidence interval error ellipsoids reported in the NTXES catalog, the differences in earthquake locations from previously published versions of the NTXES catalog, and the history of injection activities in the FWB. The digital version of the NTXES catalog is also included.

Introduction

Starting in late 2008, earthquakes within the Fort Worth basin (FWB), Texas, contributed to the central United States increased seismicity rates after the late-2000s (Frohlich *et al.*, 2010, 2016; Ellsworth, 2013; Weingarten *et al.*, 2015). Studies of individual earthquake sequences in the basin link activity, with varying degrees of certainty, to wastewater injection activities associated with unconventional shale-gas development (Frohlich *et al.*, 2010, 2011; Frohlich, 2012; Reiter *et al.*, 2012; Justinic *et al.*, 2013; Hornbach *et al.*, 2015; Scales *et al.*, 2017; Ogwari *et al.*, 2018). Seismogenic faults in the basin are steeply dipping, basement-seeded, northeast–southwest-trending normal faults (Magnani *et al.*, 2017; Quinones *et al.*, 2018; Fig. 1b) and have deformation limited to >300 Ma resolved using formation offset in seismic

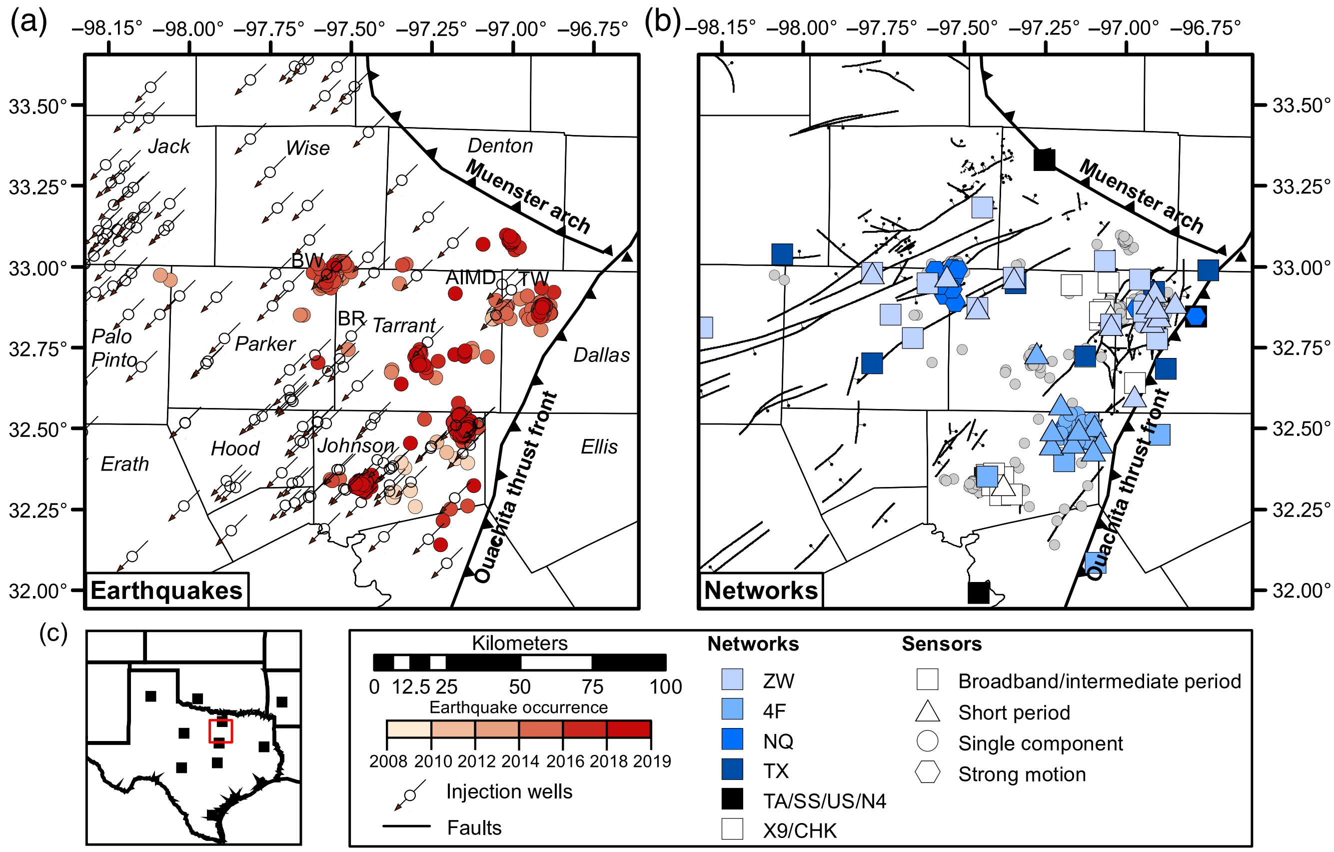

Figure 1. (a) Map view showing the locations of the North Texas Earthquake Study (NTXES) earthquakes as circles shaded by the time of their occurrence along with the locations of wastewater wells (arrows) in the basin that were active during the period of observation. County names (italics) and important well locations such as the Bond Ranch (BR), Briar Well (BW), Trigg Well (TW), and A1MD well are also labeled. (b) Map view showing the locations of all stations that were used to locate the NTXES earthquakes shaded by their network codes and the symbols of which represent the station's sensor type. The locations of the NTXES earthquakes (light gray circles) are also shown. Faults interpreted from proprietary seismic reflection data (P. H. Hennings *et al.*, unpublished manuscript, 2019; see Data and Resources). (c) General map view showing the locations of regional United States and Transportable Array (TA) stations used to locate some NTXES catalog earthquakes along with the highlighted study area (box). The color version of this figure is available only in the electronic edition.

reflection data (Magnani *et al.*, 2017). Some, but not all, of the larger magnitude earthquakes occur near wastewater disposal wells. Compilations of injection data and estimates of regional pore-pressure changes in the FWB (i.e., Gono *et al.*, 2015; Hornbach *et al*, 2016), however, need to be linked to a more complete documentation in time and space of earthquakes to holistically understand the evolution of the subsurface system. In addition, the Dallas–Fort Worth (DFW) metropolitan area (population >6 million) overlies the eastern seismogenic FWB, and a comprehensive catalog (ComCat) of FWB earthquakes provides better data for hazard and risk assessment and regulatory decisions.

The FWB is a foreland basin with a history of oil and gas production activity dating back to the early twentieth century (Pollastro *et al.*, 2007; Fig. 1). The majority of faults within the basin that have been interpreted from drilling and seismic reflection data have strikes that align well with the strikes of the major basin boundaries (e.g., Ewing, 1990; Pollastro *et al.*, 2007; Magnani *et al.*, 2017; P. H. Hennings *et al.*, unpublished manuscript, 2019; see Data and Resources). Earthquakes are limited to the northeast portion of the FWB (Fig. 1a). Here, the Barnett Shale formation has served as the primary shale-gas producing unit since 2004 (Pollastro *et al.*, 2007), and wastewater associated with this production is primarily injected into the underlying Ellenburger dolomitic limestone formation (Hornbach *et al.*, 2016). The Ellenburger lies in unconformity atop the crystalline Precambrian basement (Fig. 2a). A complete mapping of basement-seeded faults remains data limited; faults shown in this article come from recent updated compilation by P. H. Hennings *et al.* (unpublished manuscript, 2019; see Data and Resources).

Five hypocenter catalogs provide information on earthquakes in the FWB. The catalog of record, the U.S. Advanced National Seismic System (ANSS) ComCat, reports midmagnitude ($M \geq 3$) earthquakes consistently through time after 1973, but uncertainty in space can be on the order of 5–15 km. The Frohlich *et al.* (2016) historic Texas earthquake catalog provides information before 1973. Neither of these catalogs contains reliable reported

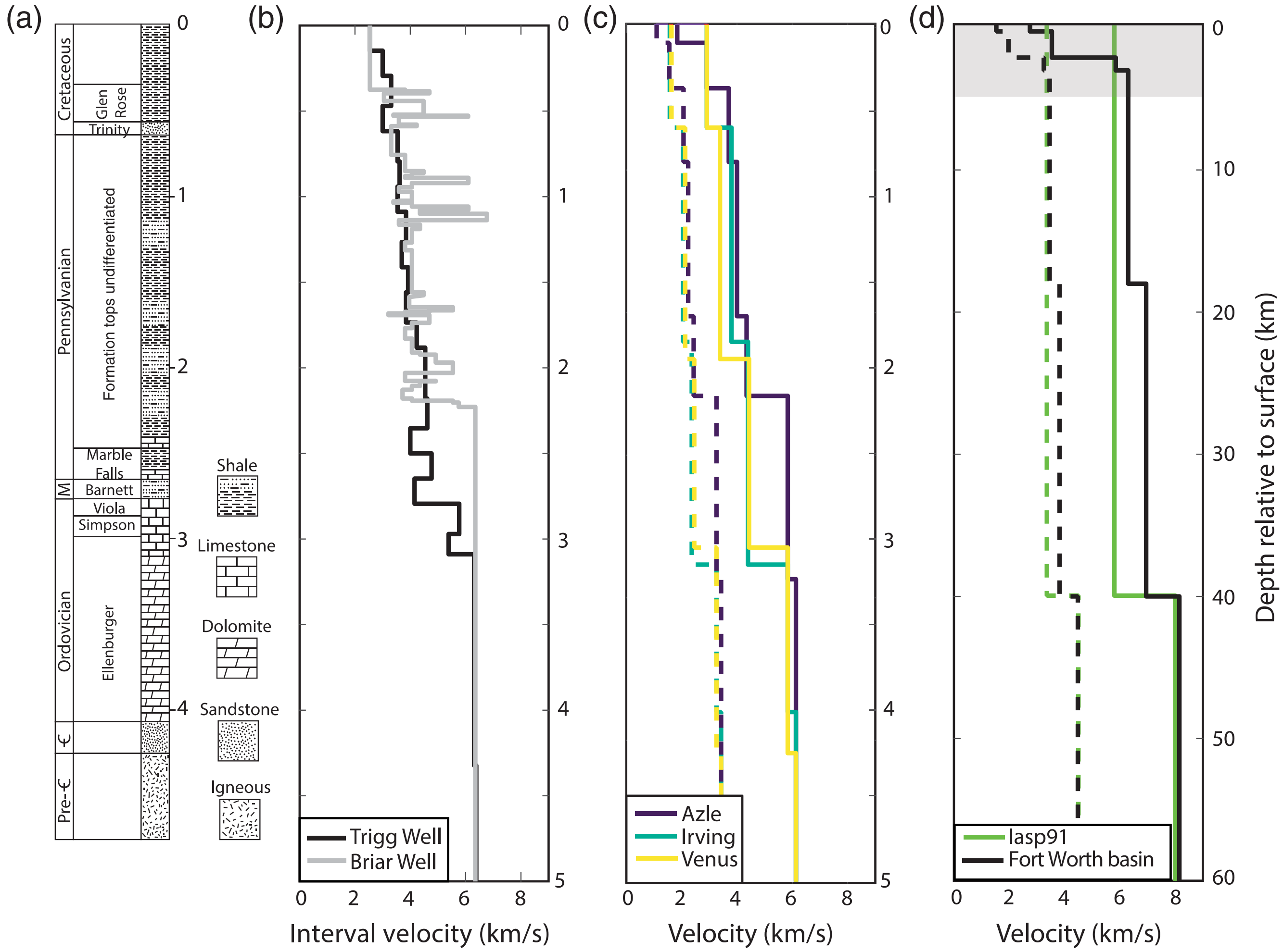

Figure 2. (a) Stratigraphic column created using data collected from the Trigg Well site. (b) Interval velocity models created using data collected from the Trigg and Briar Well sites. (c) 1D local *P*- (solid lines) and *S*-wave (dashed lines) velocity models used to locate earthquakes within the Azle, Irving–Dallas, and Venus sequences. (d) 1D regional *P*- (solid lines) and *S*-wave (dashed lines) velocity models used to locate earthquakes within the Fort Worth basin (FWB) that occur outside the three previously mentioned sequences. The upper 5 km of the regional velocity models, which is similar to the local 1D velocity models, is highlighted (gray area). The color version of this figure is available only in the electronic edition.

earthquakes in the FWB east of the Bend Arch before October 2008. Frohlich (2012) reported small-magnitude earthquakes (M < 3) in the basin using the Earthscope Transportable Array (TA) from 2009 to 2011. Between 2008 and 2019, Southern Methodist University (SMU) operated three temporary seismic networks deployed more than five named seismic sequences in the basin (Frohlich *et al.*, 2011; Justinic *et al.*, 2013; DeShon *et al.*, 2018) but focused publication of individual earthquake sequence catalogs over discrete time periods. The North Texas Earthquake Study (NTXES) catalog presented herein and included within Ⓔ Dataset S1 (available in the supplemental content to this article) reports all seismicity recorded by the temporary networks operated by SMU during the 2008–2018 period. Finally, beginning in 2017, SMU operations were combined with the Texas Seismic Network (TexNet) such that the NTXES catalog overlaps in time and space with the statewide publicly available catalog (Savvaidis *et al.*, 2019).

The NTXES catalog uses a combination of local and regional stations within the basin and a standardized approach to earthquake location and magnitude calculations. The NTXES catalog is composed of autodetected and manually reviewed earthquakes located using the GENLOC location algorithm (Pavlis *et al.*, 2004) in conjunction with local and regional 1D velocity models generated using data from well logs collected from within the FWB. We report formal uncertainties for all earthquakes in the catalog. A new regional attenuation curve constrains the local magnitudes reported in the NTXES catalog. The NTXES catalog is combined with the more temporally complete ComCat to investigate the relationship between earthquakes, faults, and wastewater injection in the FWB and explore magnitude–time relationships along individual faults and within the basin. Finally, we examine the relationship between injected wastewater rates and seismicity and discuss far-field versus near-source triggering effects of fluid injection in the basin and the possible role fluid injection activities had on the Irving–Dallas sequence, the primary cause of which is still under investigation.

Methodology for the NTXES Catalog

SMU has operated temporary seismic stations in the FWB since 2008 (Frohlich *et al.*, 2011; Justinic *et al.*, 2013) and since 2013 the local networks appear under the auspice of the NTXES, as summarized by DeShon *et al.* (2018). Continuous waveform data from all networks are archived without embargo or restriction, including currently operating stations in near-real time (see Data and Resources). The networks consist of a mix of short-period, broadband, and strong-motion stations and station locations reflect the complex history of deployment in rapid response mode (DeShon *et al.*, 2018; Fig. 1b). The resolution in time and space of the resulting NTXES hypocenter catalog reflects this complexity. Early studies using the SMU temporary networks in 2008–2010 used different location methodologies and velocity models (Frohlich *et al.*, 2010, 2011; Janská and Eisner, 2012; Reiter *et al.*, 2012; Justinic *et al.*, 2013) than later studies, which focused on stations deployed in and after 2013 (Hornbach *et al.*, 2015; Scales *et al.*, 2017; Ogwari *et al.*, 2018; Quinones *et al.*, 2018). In total, there are five well-studied earthquake sequences, here referred to by year and place name of significant first or largest event: 2008 DFW Airport (Frohlich *et al.*, 2010, 2011; Janská and Eisner, 2012; Rieter *et al.*, 2012; Ogwari *et al.*, 2018), 2009 Cleburne (Justinic *et al.*, 2013), 2013 Azle–Reno (Hornbach *et al.*, 2015; Quinones *et al.*, 2018), 2015 Dallas–Irving (Magnani *et al.*, 2017; Quinones *et al.*, 2018), and 2015 Venus (Magnani *et al.*, 2017; Scales *et al.*, 2017; Quinones *et al.*, 2018). Here, we joined all data into a single data processing stream to ensure methodological consistency and additionally report all earthquakes rather than only low-uncertainty events associated with specific earthquake sequences.

Hypocenter Determination

We use Antelope Environmental Monitoring software and underlying relational database for archiving and analysis of the temporary seismic network data. Analysis uses the offline batch-processing mode, and no real-time analysis operations were implemented. The 2008–2011 networks were not telemetered, and although stations post-2013 were, SMU did not have the staff capabilities or reporting authority to provide real-time earthquake catalogs.

From 2013 to present, batch processing 24 hr in arrears includes autodetection and association of *P*- and *S*-wave first arrivals followed by manual review of associations and raw waveforms to identify small earthquakes. A multifrequency short-term average over long-term average autodetector (dbdetect) tuned to find impulsive local distance earthquakes feeds into an event associator set to use a spatial grid-search method with the iasp91 global velocity model (dbgrassoc). In practice, autodetection and association set to optimize identification across the network can miss emergent or nodal arrivals, trigger incorrectly on a prominent *P*-to-*S*-converted phase that mixes with first-arriving *S* on some stations, and do not capture all microseismicity ($M < 1$) associated with swarm activity in some sequences. The network itself exhibits high noise levels inherent to rapid installation within a sedimentary basin and major metropolitan area (discussed in DeShon *et al.*, 2018). Thus, all continuous data are subsequently manually reviewed by a trained analyst to correct autodetections and add additional phase onsets. At this stage, all *P*-wave first-motion data are entered into the database. The analyst assigned phase-pick uncertainties associated with these manually reviewed phases are conservatively estimated to be within 0.01–0.04 s for *P*-phase picks and 0.02–0.08 s for *S*-phase picks depending on factors such as the impulsiveness of the phase arrivals and the sampling rates of the observing stations (100 or 200 samples per second).

Event review takes place within the analyst location software (dbloc2), and we use GENLOC location algorithms, which is a modified version of the Gauss–Newton inversion method meant for single-event location applications (Pavlis *et al.*, 2004). The GENLOC programs allow for multiple 1D velocity models to be interactively tested resulting in multiple origin locations and times stored for a given event. Reported formal uncertainties include origin time and a 68% confidence error ellipsoid in space and are derived from the covariance matrix in the inverse solution (Pavlis *et al.*, 2004). The median standard error of observation (sdobs) value, which is defined as the sum of the square of the phase arrival-time residuals divided by the number of degrees of freedom, is also stored by origin. For the NTXES catalog, we provide the preferred solution for each event, discussed in the Velocity Models section, and the 68% confidence error ellipsoids are provided as the ellipsoid major axis length and strike, minor axis length, depth axis length, and origin time error (see the Ⓔ supplemental content).

Velocity Models

The 1D velocity structure of the basin is derived from a combination of available geologic, well-log, and reflection data. The FWB stratigraphy summarized in Pollastro *et al.* (2007) provides the basic geology to inform 1D velocity model design (Fig. 2a). Figure 2 is plotted relative to surface, with mean elevation of ~235 m above sea level. Most significantly, the basin deepens from southwest to the northeast, as reflected in the top of the Ellenburger occurring ~1.3 km below sea level (bsl) in Parker County to more than 2.7 km under Dallas County (e.g., Pollastro *et al.*, 2007; Hornbach *et al.*, 2016; Smye *et al.*, 2019; see Fig. 1a for place names). A recent compilation of interpreted well-log data across the FWB provides thickness estimates of the Barnett and Ellenburger formations and estimates for the top of the crystalline basement near each earthquake sequence (Smye *et al.*, 2019). We use sonic logs (Fig. 2b) to constrain *P*- and *S*-wave velocities. The Trigg Well (Geotechnical Corporation, 1964), located in Tarrant County near the DFW Airport and Irving–Dallas earthquake sequence, and the Briar saltwater disposal (SWD) well, located in Wise near the Azle–Reno sequence, provide sonic logs constraining compressional wave interval velocity through the basin sedimentary units and are in general agreement (Fig. 2b). The wells also reflect the basin dip; the western Briar Well has a significant velocity jump at 2.2 km and the Trigg Well at ~3 km below surface reflecting the top of the Ellenburger formation. Dipole sonic logs available at the Bond Ranch SWD well, in western Tarrant County near Azle–Reno, and the A1MD SWD well, near the DFW Airport, suggest V_P/V_S of 1.72 for the Ellenburger and crystalline basement, ranges of 1.82–1.89 through the sedimentary package, and a return to 1.73 in the upper 500 m. Not many wells drill to top of basement, and sonic-log data do not indicate a significant velocity contrast between the Ellenburger and crystalline basement. Seismic reflection data in the basin (e.g., Magnani *et al.*, 2017) and the updated FWB stratigraphic model (Smye *et al.*, 2019) confirm an Ellenburger thickness of ~1 km. We use the Briar and Bond Ranch well data to set a 1D model for the Azle region and use the Trigg and A1MD data for DFW Airport, Irving–Dallas, Venus, and Cleburne sequences (Fig. 2c). Previous studies of the Cleburne and DFW Airport relied on only Trigg well data (Frohlich *et al.*, 2011; Justinic *et al.* 2013).

Well-log data do not constrain the very shallow (<0.5 km) or deep (>5 km) velocity structure required for accurate hypocenter location. Ambient-noise analysis of a 10-day deployment of 130 10 Hz vertical-component nodes, deployed near Azle (DeShon *et al.*, 2018), yields Rayleigh phase velocities between 0.3 and 0.9 s, which are then inverted for 1D V_P and V_S (Sufri *et al.*, 2018). These data constrain the upper 100 m of the Azle 1D velocity model (Fig. 2b) but were not extrapolated to the other 1D models. TA automated receiver functions place Moho depth between 37 and 42 km in and near the FWB with a V_P/V_S range of 1.65–1.81 (Data and Resources); we set Moho to 40 km. Frohlich *et al.* (2011) incorporated a midcrustal boundary at 18 km to best model arrivals from DFW Airport earthquakes and regional refraction studies across the Ouachita thrust front show a midcrustal boundary in Laurentia craton between 20 and 22 km (Keller and Hatcher, 1999). We take the velocities proved by Keller and Hatcher (1999) with midcrustal boundaries between 15 and 25 km, and we find that 18 km best fits first-arrival times on FWB stations. We adopted the midcrust and lower crust velocities for all 1D models (Fig. 2d). When an earthquake occurs away from a known monitored sequence, we adopt the FWB regional velocity model (Fig. 2d). Models are provided in Ⓔ Table S1 and every earthquake is reported with the associated velocity model in Ⓔ Dataset S1.

Magnitude Determination

We determine the magnitude scaling functions for the FWB and surrounding region using local and regional recordings of earthquakes in the basin between 2013 and 2018. Whereas at close epicentral distances (<100 km), earthquakes are recorded by broadband, short-period, and strong-motion sensors, at regional distances (>100 km) the earthquake signals are best recorded by the broadband stations. At very close epicentral distances (<50 km), the dominant recorded phase is the first-arriving *S* wave; however, at epicentral distances beyond 50 km, the *Lg* wave begins to dominate the signal (Nuttli, 1973; Atkinson and Boore, 2013). Local magnitude is expressed as

$$M_L = \log_{10} A(\Delta) - \log_{10} A_0(\Delta) + c, \quad (1)$$

in which $\log_{10} A(\Delta)$ is the base-10 logarithm of the peak amplitude (in millimeters) on a Wood–Anderson seismometer measured at some epicentral distance Δ (in kilometers), and c is a station correction term that is not applied in this study (Richter, 1935). The $\log_{10} A_0(\Delta)$ term is a distance-scaling factor that is determined by constraining the zero point of the magnitude scale to a hypothetical Wood–Anderson instrument. For instance, at 100 km from the epicenter, the peak amplitude of an M_L 3.0 earthquake is equal to 1 mm as defined by Richter (1935). With a c-value of 0, the distance-scaling factor can thus be expressed as

$$\log_{10} A_0(100) = \log_{10} A(100) - 3 = \log_{10} 1 - 3. \quad (2)$$

We empirically derive the $\log_{10} A_0(\Delta)$ term by first convolving instrument-corrected waveforms with a Wood–Anderson instrument response. We then sample events with at least one recording station at an epicentral distance of ~100 km, which is then used as a normalization station for that earthquake. Peak amplitudes are derived from the greater of the two horizontal-component waveforms bandpass filtered between 0.1 and 5.0 Hz (Fig. 3), following the original practice described by Richter (1935) and adopted by U.S. Geological Survey for computation of M_L (Patton *et al.*, 2016). Normalization of all stations for each event to the recording at ~100 km conditions each earthquake to M_L 3.0. A previous local magnitude scale derived using FWB data calibrated M_L to the ANSS ComCat reported m_{b_Lg} following the method of Walter *et al.* (2016) and Scales *et al.* (2017). The Scales *et al.* (2017) relation has been adopted as M_L for the TexNet (Savvaidis *et al.*, 2019).

Here, we derive an attenuation curve using recordings of earthquakes reported in the ComCat, following Scales *et al.* (2017), but normalized as described earlier. Events reported in the ComCat exhibit good signal-to-noise ratio at regional broadband stations (Fig. 1c) and at broadband and strong-motion stations within the basin. In addition, we use recordings from the TA between 2008 and 2011. The initial earthquake set (black circles, Fig. 3) yields primarily

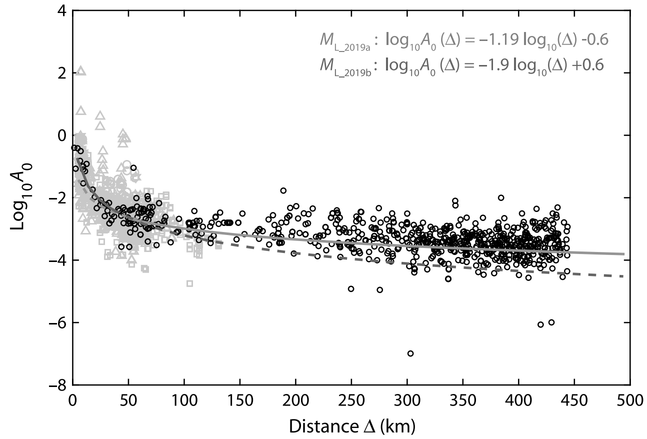

Figure 3. Attenuation curves created for the FWB. Light gray symbols represent peak amplitudes normalized to a station located 50 km from the epicenter; symbol shape follows Figure 1. Black circles represent peak amplitude normalized to a station located 100 km for earthquakes reported in the comprehensive catalog (ComCat). The dashed gray line best fits small-magnitude earthquakes recorded by the NTXES networks, and the solid gray line best fits regional broadband data. Hence, we adopt M_{L_2019b} attenuation relation for data recorded at <50 km and the M_{L_2019a} for data at >50 km (solid portions of lines).

regional distance data out to 400 km. The best-fit attenuation curve (gray line, Fig. 3) models amplitude of first-arriving *S*, transition to *Lg*. This curve fit represents the attenuation of the *Lg* waves and could also be considered an m_{b_Lg} magnitude equivalent. This station–event dataset is identical to Scales *et al.* (2017), but the change in normalization significantly reduces scatter in the amplitudes at individual stations (Scales *et al.*, 2017) and matches ComCat m_{b_Lg} without need of additional correction. The resulting M_L relationship is

$$M_{L\_2019a} = \log_{10} A_0(\Delta) - 1.19 \log_{10}(\Delta) - 0.6. \qquad (3)$$

The NTXES catalog contains many very small earthquakes that were not recorded at 100 km or on the broadband and strong-motion sensors originally analyzed. We found that the M_{L_Scales} and M_{L_2019a} relationship significantly overestimated peak amplitudes for local stations (<50 km). Therefore, we normalize the short epicentral distance peak amplitudes (light gray symbols, Fig. 3) using stations at 50 km distance and then adjust the amplitude values to the zero point based on the 100 km normalization distance data. The resulting M_L is

$$M_{L\_2019b} = \log_{10} A_0(\Delta) - 1.9 \log_{10}(\Delta) + 0.6. \qquad (4)$$

This attenuation curve calculates M_L that match the m_{b_Lg} well for earthquakes at local distances (<50 km) but overestimates the magnitudes of earthquakes at regional distances (Fig. 3). The scatter in the plot is attributed partly to stations' site effect and radiation pattern.

The NTXES catalog reports a single magnitude per earthquake calculated using the Antelope software magnitude calculator dbevproc. Any event reported within the NTXES catalog recorded using only stations within the 50 km epicentral distance limit uses the M_{L_2019b} attenuation curve function, which is included as a modification to the dbevproc parameter file. Meanwhile, if an event recorded within the FWB uses many regional stations at distances exceeding 50 km, then the M_{L_2019a} attenuation curve function applies. However, no events reported in the 2008–2018 NTXES catalog use regional phases because the 1D velocity models are designed for local network data, and hence regional phases are not integrated into the Antelope database, even for larger earthquakes. In practice, all M_L reported in the NTXES catalog through 2019 reflect M_{L_2019b}. Uncertainty is estimated to be on the order of 0.1–0.3 units. Ⓔ Figure S1 shows the crossplot between M_{L_2019b} and m_{b_Lg} for earthquakes reported in the NTXES and ComCat catalogs, respectively.

Results

Earthquake Catalog

The seismicity reported in the NTXES catalog describes individual earthquake sequences along linear features identified as faults and contains individual earthquakes scattered in time that are not easily ascribed to known faults (Fig. 4). The catalog describes two separate time periods of seismic monitoring activity: 2008–2010 and post-2013 (Fig. 4). In the NTXES catalog, we identify nine active earthquake sequences on discrete faults described by their location and year of initial activity here: DFW Airport (2008), Cleburne (2009), Azle–Reno (2013), Irving–Dallas (2015), Venus (2015), Haslet (2015), Lake Lewisville (2017), Fort Worth (2017), and west Cleburne (2018). Of these, Lake Lewisville, Fort Worth, and west Cleburne have not been previously reported and have only one or two monitoring stations within a 10 km hypocentral distance. These three sequences are shown in cross section in Figure 5 but have significant depth uncertainty compared with the well-recorded Azle–Reno, Irving–Dallas, and Venus sequences. Figure 6 shows the formal uncertainties for the NTXES catalog, subdivided by the three significant post-2013 event sequences, and all earthquakes located using the regional velocity model. Taking the entire dataset, median values for major, minor, and depth axes are <0.4 km and median origin time error is 0.04 s. The residual measure, sdobs, also has a median of 0.04 s. Individual event uncertainties can range higher, however, and we provide formal error estimates for each event in Ⓔ Dataset S1.

The majority of earthquakes in the FWB are occurring within the Precambrian granitic basement (Fig. 5b–g). However, a portion of earthquakes within the Azle–Reno and regionally located sequences locate within the Ellenburger formation (Fig. 5b,e–g). Whereas the shallower Azle–Reno events are associated with an antithetic feature near the main

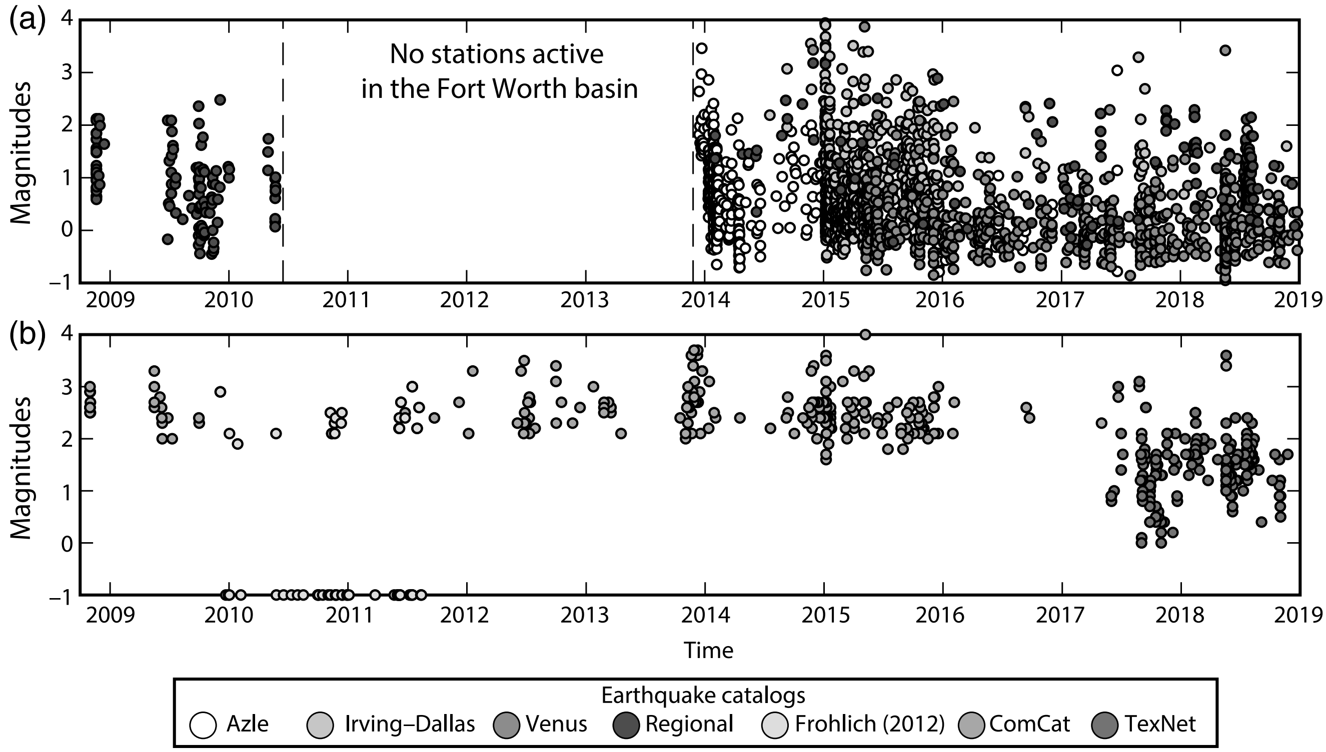

Figure 4. (a) Magnitude versus time plot of the NTXES catalog separated into the Azle, Irving–Dallas, Venus, and regional subgroups (dashed lines indicate time period in which there were no active stations within the FWB). (b) Magnitude versus time plot of the earthquakes located within the FWB from the Frohlich (2012), ComCat, and Texas Seismic Network (TexNet) earthquake catalogs.

fault (Hornbach *et al.*, 2015), the shallower events in the regionally located sequences are likely an effect of larger depth uncertainties because of a lack of close hypocentral distance stations.

Each of the earthquake sequences within the FWB exhibits swarm-like behavior rather than resembling mainshock–aftershock sequences. Figure 4 shows the magnitude versus time distribution of all earthquakes recorded within the FWB separated by reporting catalog. The characteristic distribution of seismicity over time associated with each individual sequence in the FWB is a relatively short period (6–12 months) of peak seismicity followed by a steep decline in subsequent seismicity. However, overall basinwide seismicity rates have remained steady since the onset of recorded seismicity in the FWB in 2008. Thus, the gap in recorded seismicity within the NTXES catalog from 2010 to 2013 is actually a gap in local seismic monitoring capabilities rather than seismic activity.

Magnitude Distribution

All NTXES catalog magnitudes are calculated using the $M_{\mathrm{L\_2019b}}$ attenuation curve function (Fig. 3). The overall magnitude range of earthquakes within the NTXES catalog is M_L − 1.0 to M_L 4.0, although the magnitude range of each individual sequence varies. The differences in the number of stations, station geometry, and overall noise levels across the sequences described in the NTXES catalog led to large variations in the degree of catalog completeness across the nine sequences in the FWB.

There is spatial variation in the magnitude of completeness (M_c) and *b*-values of the sequences described within the NTXES catalog. The NTXES catalog is divided into four subgroups; the three significant post-2013 sequences being the Azle–Reno, Irving–Dallas, and Venus sequences and the sequences located using a regional velocity model hereafter referred to as the regional sequences. M_c and *b*-values are calculated for each subgroup using the 90% goodness-of-fit method (Wiemer and Wyss, 2000) and the maximum-likelihood estimation method, respectively (Bender, 1983). We observe a wide range in M_c values across the subgroups from $M_\mathrm{c} = 0.0$ for the Venus subgroup to $M_\mathrm{c} = 2.1$ for the regional events subgroup (Fig. 7). The higher M_c value for the regional events can be attributed to a lack of local stations to monitor the small-magnitude events. Meanwhile, the variation in M_c values across the three locally monitored sequences in the NTXES catalog can be attributed to a nonoptimal initial network geometry in the case of the Azle–Reno sequence and to elevated noise levels in the Irving–Dallas sequence, which is embedded in the metroplex (DeShon *et al.*, 2018). The *b*-values also vary across the subgroups from 0.67 for the Irving–Dallas subgroup to 1.01 for the Azle subgroup (Fig. 7). The lower *b*-values calculated for the Irving–Dallas and Venus subgroups are likely due to a

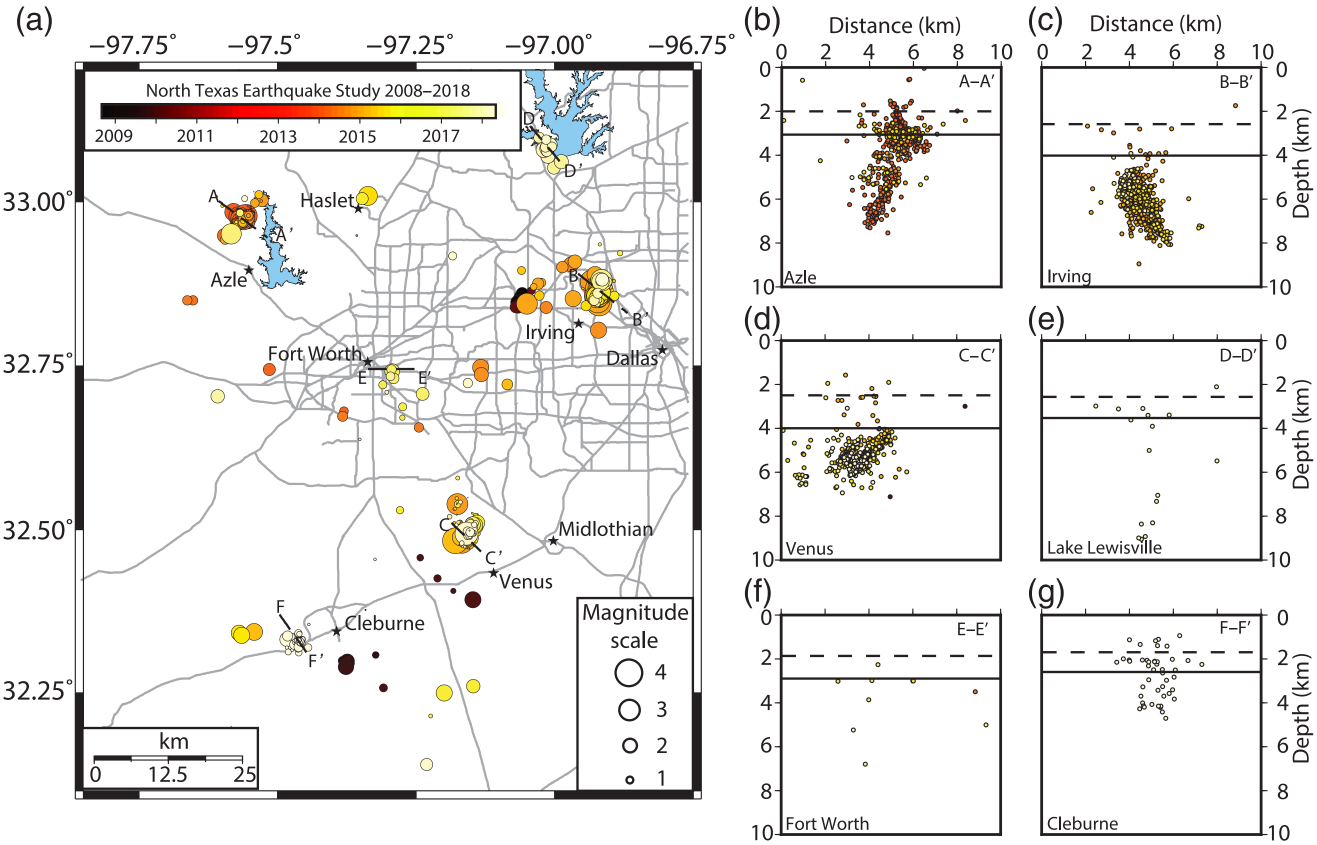

Figure 5. (a) Map view of the NTXES study area showing the locations of all earthquakes in the catalog shaded by their time of occurrence and scaled by their magnitude. The major roads and highways (gray lines) in the region are also shown. Lettered dashed lines represent profile lines used to create the separate cross-sectional views for each named sequence. (b–g) Cross-sectional views of each named sequence site using the same occurrence timescale. The depths of the top of the Ellenburger (dashed lines) and basement (solid lines) at each sequence site are also shown. The color version of this figure is available only in the electronic edition.

variety of factors such as M_c uncertainties (Woessner and Wiemer, 2005), missing early lower magnitude events before instrument deployment (Scales *et al.*, 2017), or noise-level issues (DeShon *et al.*, 2018). In addition, using the same methodology, we calculated that the 2008–2018 ComCat catalog of FWB earthquakes has an M_c value of 2.6 and b-value of 1.25 (Fig. 7). Last, we calculated the b-value for the NTXES catalog using the M_c value from the regional events subgroup (2.1) and found a value of 0.74.

Location Changes from Prior Catalogs

The seismicity reported within the NTXES catalog for the DFW Airport, Cleburne, Azle–Reno, Irving–Dallas, and Venus areas has been presented and discussed in prior publications but now have some differences in earthquake locations to the NTXES catalog presented here. The NTXES catalog locations are different than in prior publications because of the updating of velocity models used for earthquake location (Fig. 2). Previous publications presented the original velocity models used to calculate earthquake locations were based on then-available well-log and geologic data. The updated velocity models have been supplemented with newly available sonic log, seismic reflection, ambient-noise tomography, and geologic data as described in the Velocity Models section. Overall, there is little change in the earthquake hypocenter locations with median changes (with 50% confidence error values) of 0.00 ± 0.07, -0.01 ± 0.07, and 0.00 ± 0.19 km for the latitude, longitude, and depth, respectively, from the prior published catalogs to those presented here. In addition, origin time differs only slightly with a median change of -0.01 ± 0.03 s (Ⓔ Fig. S3). Therefore, although the earthquake locations have slightly changed with the updating of the velocity models, the fault structures described by the distributions of the earthquake locations at each sequence site are similar. Thus, previous interpretations of fault geometries and earthquake location distributions remain valid.

Discussion

Earthquakes and Faults

The majority of active faults in the FWB are northeast–southwest-trending normal faults, which are concentrated in the northeast portion of the basin (Fig. 1b). Prior studies focusing on the three most significant post-2013 FWB

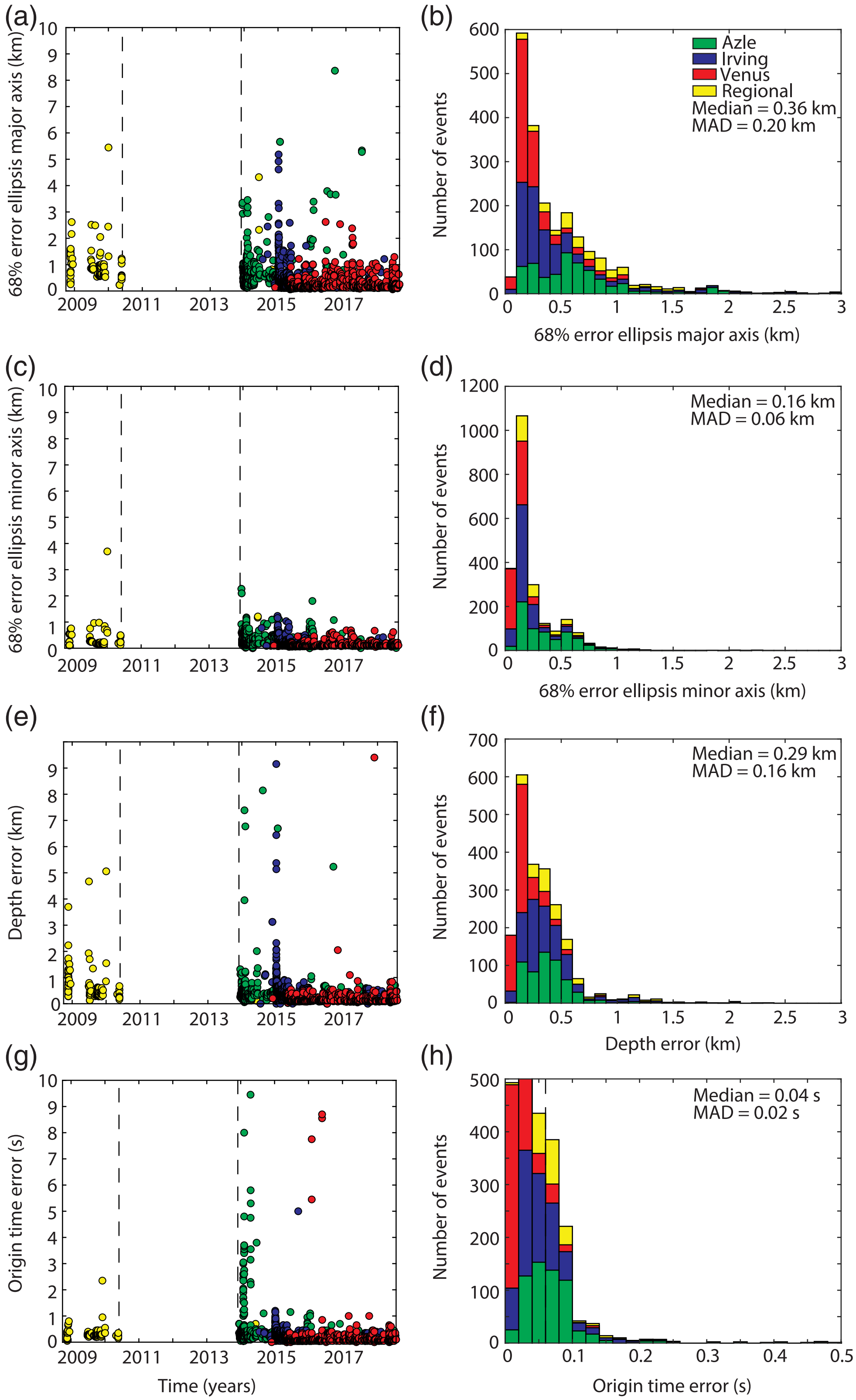

Figure 6. (a,c,e,g) Scatter plot views showing the lengths of the (a) major and (c) minor axes of the 68% confidence error ellipsis, (e) associated depth errors, and (g) origin time errors of the NTXES catalog earthquakes versus time (dashed lines indicate time period in which there were no active stations within the FWB). Each earthquake is represented by a separate circle shaded by its sequence. (b,d,f,h) Stacked histograms showing the distributions of the same four error parameters in the same order for the NTXES catalog. Each sequence's contribution to the cumulative distribution of location errors is shown. The median and median absolute deviation (MAD) values for each location parameter are also shown. The color version of this figure is available only in the electronic edition.

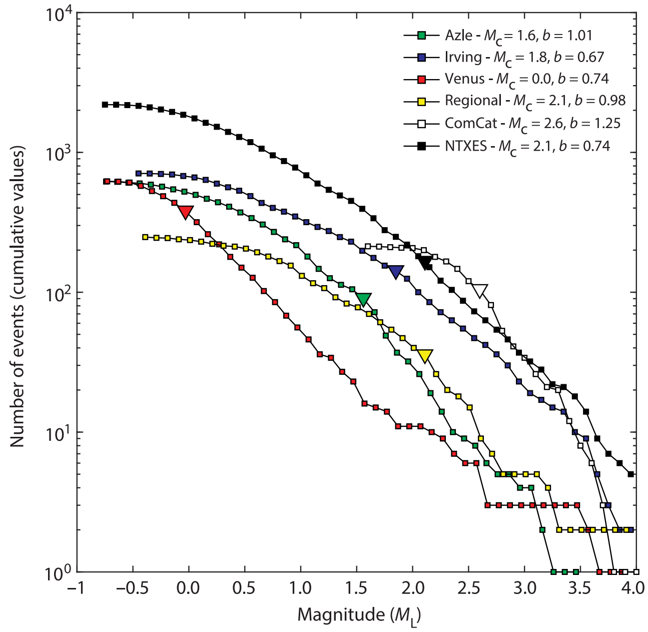

Figure 7. Gutenberg–Richter plot showing the magnitude of completeness (M_c) and b-values for each subsection of the NTXES catalog, the NTXES catalog as a whole, and the National Earthquake Information Center catalog of FWB events for comparison. The M_c values are represented by the inverted triangles in the plot. The color version of this figure is available only in the electronic edition.

sequences have used the NTXES catalog to interpret fault geometries and deformation histories of the active faults in the FWB through the use of focal mechanism (Quinones *et al.*, 2018) and seismic reflection data (Magnani *et al.*, 2017). The focal mechanisms generated from the NTXES catalog described the source faults of each of these sequences as steeply dipping normal faults with strikes of ~40° and dips of between 56° and 70° (Quinones *et al.*, 2018). Meanwhile, seismic reflection data collected across the Venus and Irving–Dallas sequence sites revealed a lack of vertical displacement on the faults at both sites in rocks younger then ~310 Ma (Magnani *et al.*, 2017). This implies that the faults at both sites remained inactive since the Pennsylvanian. Subsequently, additional proprietary seismic reflection data collected across the basin revealed more widespread northeast–southwest-trending faulting in the northeast portion of the FWB. Also, the majority of northeast–southwest-trending faults in the FWB are considered optimally oriented for failure with high-slip potentials within the local and regional stress fields described by the focal mechanisms and borehole breakout data collected from the basin (Quinones *et al.*, 2018; P. H. Hennings *et al.*, unpublished manuscript, 2019; see Data and Resources). In each study, the NTXES catalog was essential in providing proper constraints and interpretations of the resulting imaged fault structures in the FWB.

The NTXES catalog contains a record of seismicity occurring within the previously undocumented Lake Lewisville (2017), Fort Worth (2017), and west Cleburne (2018) sequences. The earthquakes within these sequences are located using the regional velocity model with data collected by a combination of TexNet- and SMU-operated stations, although no dedicated local networks have been installed at any of these sequence sites. Thus, fewer earthquakes have been detected within these sequences, and those that have been located have higher associated depth uncertainties. Because of these issues, we cannot provide the same degree of fault interpretation for these three sequences compared with the other post-2013 sequences. The Lake Lewisville sequence consists of 17 earthquakes with depths ranging from 2 to 9.5 km, which appear to occur along a steeply dipping northeast–southwest-trending fault plane (Fig. 5e). The Fort Worth sequence consists of only nine detected earthquakes ranging in depth from 2 to 7 km (Fig. 5f). We have not provided a fault interpretation for the Fort Worth sequence because of the lack of associated hypocenter locations. The west Cleburne sequence is the most recent to become active; however, its associated earthquake count has already surpassed those of the Lake Lewisville and Fort Worth sequences. The west Cleburne sequence earthquakes have the highest location uncertainty values in the NTXES catalog because of a sizable network azimuthal gap and the lack of local stations for depth control. The earthquakes in west Cleburne range in depths from 1 to 5 km and appear to describe a steeply dipping north–south-trending fault similar in orientation to the fault described by the original Cleburne sequence (Fig. 5g, Justinic *et al.*, 2013). This north–south-trending fault interpretation means this fault would not be optimally oriented for failure within the previously reported FWB stress regimes (Lund Snee and Zoback, 2016; Quinones *et al.*, 2018); however, seismic reflection and well head data interpretation also point to a north–south-trending fault at this location (P. H. Hennings *et al.*, unpublished manuscript, 2019; see Data and Resources).

Earthquakes and Injection Data

The seismicity occurring within the FWB is part of the larger trend of increasing amounts of induced seismicity within the central United States, which has been associated with fluid injection activities. Pore-pressure diffusion associated with fluid injection activities is hypothesized to be the primary mechanism driving induced seismicity within the FWB (Frohlich *et al.*, 2016; Hornbach *et al.*, 2016) and throughout the central United States (e.g., Keranen and Weingarten, 2018). Monthly volumes of fluids injected into the Ellenburger formation, the main disposal unit in the basin, by SWD wells are reported by the Texas Railroad Commission and can be accessed electronically using their public database. Over the time period of October 2005 to October 2017, more than 2 billion U.S. barrels of fluids from 179 SWD wells were injected into the Ellenburger formation. When we examine an interpolated surface describing the cumulative volumes of injected fluids from 2005 to 2017, we observe that the northeast portion of the FWB is where

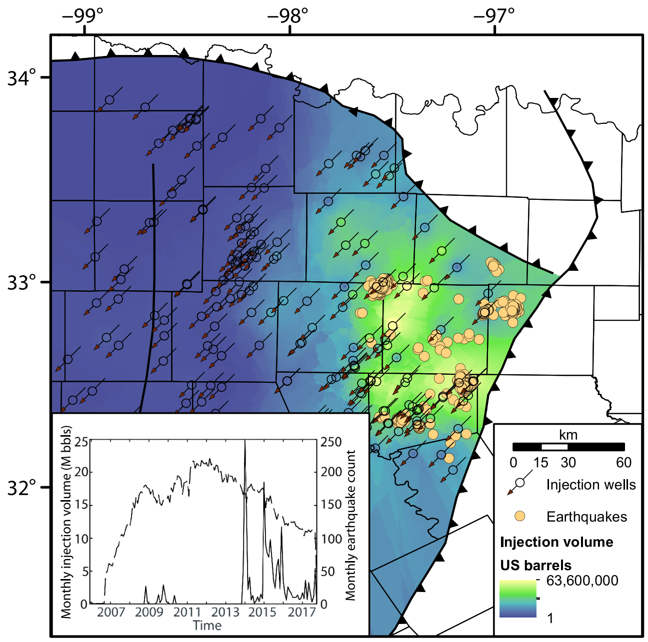

Figure 8. Map view showing the interpolated cumulative injection volumes of all fluids injected into the Ellenburger formation from October 2005 to October 2017. The interpolation was conducted using an inverse distance weighting scheme using a weighting power of 1 and using data values taken from the 10 nearest wells to each point in space. Each cell is approximately 1.94 km by 1.94 km in size. The earthquake (circles) and injection well (arrows) locations are also shown. (Inset) Plot showing the monthly injection volumes in millions of U.S. barrels (M bbls) for the FWB as a whole (dashed line) and the monthly number of earthquakes recorded within the NTXES catalog (solid line) over the same time period. The color version of this figure is available only in the electronic edition.

both the majority of injection activities and seismicity is occurring within the basin (Fig. 8). In fact, with the exceptions of the Irving–Dallas and Lake Lewisville sequences, the majority of seismicity within the FWB is occurring within 15 km of at least one injection well. The spatial proximity of these near-well sequences, along with the strong temporal correlation between the onset of seismicity and increasing injection rates within the FWB (Fig. 8, inset), suggests that pore-pressure diffusion is the main driving force for induced seismicity at these sequence sites. However, injection rates have decreased in recent years from their peak levels in 2014, mainly because of economic reasons, which do appear to coincide with lowering rates of seismicity across the FWB. Previous studies using the NTXES catalog data focusing on these near well sequences have found that pore-pressure changes associated with injection activities are significant and are the primary mechanism driving seismicity at these sites (Frohlich *et al.*, 2011; Hornbach *et al.*, 2015, 2016; Scales *et al.*, 2017; Ogwari *et al.*, 2018; Quinones *et al.*, 2018). However, stress changes associated with pore-pressure diffusion are often limited to distances close to wells (<15 km; Segall and Lu, 2015; Goebel *et al.*, 2017), leaving the question for what the main mechanisms driving seismicity at sites that are at far distances from injection wells.

Far-Field versus Near-Source Triggering

Although pore-pressure changes caused by fluid injection activities are the dominant stress change effect at near well distances, modeling results have shown that at farther distances from injection wells (>15 km), poroelastic stress changes dominate. Recent studies on stress changes associated with injection activities have focused on not only understanding direct pore-pressure changes but also on understanding the far-field effects of poroelastic stress changes (Segall and Lu, 2015; Chang and Segall, 2016; Goebel *et al.*, 2017). In the FWB, two sequences occur away from injection wells: the Irving–Dallas and Lake Lewisville sequences (Fig. 8).

Results of injection-related stress change modeling predict a crossover distance at which poroelastic stress effects become dominant over direct pore-pressure stress changes (Segall and Lu, 2015; Goebel *et al.*, 2017). However, this crossover distance is highly variable, relying on factors such as the properties of the injection unit, the injection rate, and the duration of injection activities. Prior studies sought to model pore-pressure stress changes within the FWB, focusing on the basinwide effects of injection activities (Gono *et al.*, 2015; Hornbach *et al.*, 2016; Zhai and Shirzaei, 2018) and the localized stress changes associated with injection activities at the DFW Airport (Ogwari *et al.*, 2018). Hornbach *et al.* (2016) found the Ellenburger to be overpressured by about 1.7–4.5 MPa at injection well sites in northeast Johnson county, and Zhai and Shirzaei (2018) calculated overpressure within the Ellenburger to be ~2 MPa in that same area. Ogwari *et al.* (2018) also found that injection activities increased pore fluid pressure within both the Ellenburger and basement formations in the DFW Airport area. In these studies, we observe that stress changes associated with direct pore-pressure effects are highly concentrated at close distances to the wells. Thus, it is believed that poroelastic rather than pore-pressure stress changes are the primary driving mechanism of seismicity sequences at far distance sites. However, although poroelastic stress changes are dominant over pore-pressure stress changes at far distances, the actual magnitude of the poroelastic stress changes is still lower than the near well pore-pressure effects (Segall and Lu, 2015). This leads to a larger question, still remaining to be resolved in the FWB: Would poroelastic stress changes alone be large enough to have induced slip on the far distance sequences? Previous studies attempted to calculate the slip probability and stress change necessary to induce slip of the Irving–Dallas sequence fault (Quinones *et al.*, 2018; P. H. Hennings *et al.*, unpublished manuscript, 2019; see Data and Resources). Both studies determined that the Irving–Dallas fault is an optimally oriented for failure within the given stress field (3.48 ± 2.39 MPa), but it is unclear whether poroelastic stress changes alone would be enough to induce slip on the fault.

North Texas

The FWB seismicity shares many characteristics with other induced seismicity sites occurring throughout the central United States such as primarily being concentrated near injection wells, occurring within the basement formations, and having a strong temporal correlation with increasing injection rates. Numerous catalogs of induced seismicity throughout the central United States report that the majority of seismicity is occurring along faults residing within the Precambrian basement, which typically underlies the main fluid disposal unit in the region. This pattern in induced earthquake depths has been observed in the FWB, Guy-Greenbriar (Horton, 2012), Raton basin (Rubinstein *et al.*, 2014), Oklahoma (Keranen *et al.*, 2014), southern Kansas (Rubinstein *et al.*, 2018), and Delaware basin sequence sites. This is not to say that no seismicity occurs within the units above the basement; seismicity was also recorded within the fluid disposal unit at each of the aforementioned sequence sites. These earthquake depth distributions imply that the active faults within the basement formations are either hydraulically conductive or connected to the fluid disposal formations (Chang and Segall, 2016).

Seismic reflection data collected across the Irving–Dallas and Venus regions show that the faults at each site stretch into the overlying units above the basement (Magnani *et al.*, 2017). This means that the faults themselves could act as the connection between the fluid disposal and basement units allowing for the transfer of pore pressure between them. Pore-pressure modeling work focusing on the Azle–Reno and Venus sites is ongoing; however, such modeling efforts are not currently underway for the Irving–Dallas site because of its far distance from injection wells. At present, all measurements of pore-pressure and poroelastic stress changes affecting the Irving–Dallas site come from basinwide modeling efforts, which have calculated very little to no stress changes in the Irving–Dallas area (e.g., Zhai and Shirzaei, 2018). The Irving–Dallas sequence, still the most enigmatic of the sequences, generated significant felt earthquakes within the NTXES catalog, and determining the main driving mechanism behind its seismicity will require a better understanding of how pore pressure, poroelasticity, and the injected fluids flow and diffuse throughout the FWB.

Summary

The NTXES catalog represents the most complete record of seismicity occurring within the FWB. All catalog earthquake locations are manually reviewed and calculated using the GENLOC location algorithm within the Antelope database software system. The earthquake hypocenter locations and their 68% confidence error ellipsoid information are reported within the catalog (see Ⓔ supplemental content). The 1D velocity models used for locating the FWB earthquakes were generated using a combination of geologic, well-log, ambient-noise, receiver function, and seismic reflection data collected from across the basin. All magnitudes reported in the NTXES catalog are local magnitudes calculated using new specialized regional attenuation curve functions for earthquakes located using either local or regional distance station data. As a whole, the NTXES catalog earthquakes have low location uncertainties due to the majority of events being located by dedicated local seismic networks at close epicentral distances with good azimuthal coverage. In the NTXES catalog, we identify nine separate earthquake sequences occurring along discrete steeply dipping northeast–southwest-trending normal faults located primarily within the Precambrian basement formation. The M_c of the NTXES catalog varies across the sequences because of differences in station density and network geometry; however, the overall M_c of the catalog is lower than that of other seismicity catalogs in the FWB such as the ComCat catalog. Overall, seismicity in the FWB does have a strong spatial and temporal correlation with fluid injection activities with the majority of seismicity occurring within 15 km of SWD wells. The main exceptions to this are the Irving–Dallas and Lake Lewisville sequences, which have no SWD wells within 15 km. This means that far-field rather than near-source stress changes may contribute to driving seismicity at either sequence site. Future work involving the NTXES catalog may focus more on the modeling of geomechanical stress changes associated with fluid injection activities to discern the main mechanisms driving seismicity both near and far from well distance sequence sites.

Data and Resources

All seismic data used in this study were collected as part of the North Texas Earthquake Study (NTXES) projects focusing on the study of seismicity occurring within the northeastern portion of the Fort Worth basin (FWB). These projects were conducted by Southern Methodist University (SMU) using a combination of SMU, U.S. Geological Survey (USGS), Incorporated Research Institutions for Seismology–Program for the Array Seismic Studies of the Continental Lithosphere (IRIS-PASSCAL), and Texas Seismic Network (TexNet) instruments. The data used in this study can be obtained from the IRIS Data Management Center at www.iris.edu under the Federated Digital Seismic Network codes NQ, ZW, 4F, and TX (last accessed February 2019). Transportable Array (TA) receiver function information can be accessed using the IRIS Earthscope Automated Receiver Survey (EARS) data services product at doi: 10.17611/DP/EARS.1. Injection volume information for saltwater disposal (SWD) wells in the FWB can be obtained from the Texas Railroad Commission's online public database at webapps.rrc.texas.gov/H10/h10PublicMain.do (last accessed January 2019). The TexNet earthquake catalog information can be obtained from their public online website at www.beg.utexas.edu/texnet-cisr/texnet (last accessed February 2019). The Advanced National Seismic System (ANSS) Comprehensive Catalog (ComCat) information can be obtained from the public online website at https://earthquake.usgs.gov/earthquakes/search/ (last accessed May 2019). The other information is from the unpublished manuscript by P. H. Hennings, J. Lund Snee, J. Osmond, H. R. DeShon, R. Dommisse, E. Horne, C. Lemons, and M. D. Zoback, 2019, "Injection-induced seismicity and fault slip potential in the Fort Worth basin, Texas."

Acknowledgments

The North Texas Earthquake Study (NTXES) projects were partially funded by U.S. Geological Survey (USGS) Earthquake Hazards Program Cooperative Agreements G15AC00141 and G16AC00247 to H. R. DeShon and M. B. Magnani in addition to funding provided by the Texas Seismic Network (TexNet) program at the Bureau of Economic Geology, University of Texas. The authors thank Kaylee Kaigler, Austen Klauser, Elizabeth Layton, Remi Oldham, and Mason Phillips for aid in the manual identification of phase onset times for many of the earthquakes within the NTXES catalog. The authors declare that we have no real or perceived conflicts of interest.

References

Atkinson, G., and D. Boore (2013). The attenuation of Fourier amplitudes for rock sites in eastern North America, *Bull. Seismol. Soc. Am.* **104,** 513–528, doi: 10.1785/0120130136.

Bender, B. (1983). Maximum likelihood estimation of b values for magnitude grouped data, *Bull. Seismol. Soc. Am.* **73,** no. 3, 831–851.

Chang, K. W., and P. Segall (2016). Injection-induced seismicity on basement faults including poroelastic stressing, *J. Geophys. Res.* **121,** no. 4, 2708–2726, doi: 10.1002/2015JB012561.

DeShon, H. R., C. T. Hayward, P. O. Ogwari, L. Quinones, O. Sufri, B. Stump, and M. Magnani (2018). Summary of the North Texas Earthquake Study Seismic Networks, 2013-2018, *Seismol. Res. Lett.* **90,** no. 1, 387–394, doi: 10.1785/0220180269.

Ellsworth, W. L. (2013). Injection-induced earthquakes, *Science* **341,** no. 6142, 1225942, doi: 10.1126/science.1225942.

Ewing, T. (1990). *Tectonic Map of Texas*, Bureau of Economic Geology, University of Texas, Austin, Texas.

Frohlich, C. (2012). Two-year survey comparing earthquake activity and injection-well locations in the Barnett Shale, Texas, *Proc. Natl. Acad. Sci. Unit. States Am.* **109,** no. 35, 13,934–13,938, doi: 10.1073/pnas.1207728109.

Frohlich, C., H. DeShon, B. Stump, C. Hayward, M. Hornbach, and J. I. Walter (2016). A historical review of induced earthquakes in Texas, *Seismol. Res. Lett.* **87,** no. 4, 1022–1038, doi: 10.1785/0220160016.

Frohlich, C., C. Hayward, B. Stump, and E. Potter (2011). The Dallas-Fort Worth earthquake sequence: October 2008 through May 2009, *Bull. Seismol. Soc. Am.* **101,** no. 1, 327–340, doi: 10.1785/0120100131.

Frohlich, C., E. Potter, C. Hayward, and B. Stump (2010). Dallas-Fort Worth earthquakes coincident with activity associated with natural gas production, *The Leading Edge* **29,** 270–275.

Geotechnical Corporation (1964). Deep-hole site report, Trigg no. 1, Dallas County, Texas, *Geotechnical Corporation Technical Report 64-100*.

Goebel, T. H. W., M. Weingarten, X. Chen, J. Haffener, and E. E. Brodsky (2017). The 2016 Mw5. 1 Fairview, Oklahoma earthquakes: Evidence for long-range poroelastic triggering at >40 km from fluid disposal wells, *Earth Planet. Sci. Lett.* **472,** 50–61, doi: 10.1016/j.epsl.2017.05.011.

Gono, V., J. E. Olson, and J. F. Gale (2015). Understanding the correlation between induced seismicity and wastewater injection in the Fort Worth basin, *49th US Rock Mechanics/Geomechanics Symposium*, American Rock Mechanics Association, San Francisco, California, 28 June–1 July 2015.

Hornbach, M. J., H. R. DeShon, W. L. Ellsworth, B. W. Stump, C. Hayward, C. Frohlich, H. R. Oldham, J. E. Olson, M. B. Magnani, C. Brokaw, *et al.* (2015). Causal factors for seismicity near Azle, Texas, *Nature Comm.* **6,** doi: 10.1038/ncomms7728.

Hornbach, M. J., M. Jones, M. Scales, H. R. DeShon, M. B. Magnani, C. Frohlich, B. Stump, C. Hayward, and M. Layton (2016). Ellenburger wastewater injection and seismicity in North Texas, *Phys. Earth Planet. In.* **261,** 54–68, doi: 10.1016/j.pepi.2016.06.012.

Horton, S. (2012). Disposal of hydrofracking waste fluid by injection into subsurface aquifers triggers earthquake swarm in central Arkansas with potential for damaging earthquake, *Seismol. Res. Lett.* **83,** no. 2, 250–260, doi: 10.1785/gssrl.83.2.250.

Janská, E., and L. Eisner (2012). Ongoing seismicity in the Dallas-Fort Worth area, *The Leading Edge* **31,** no. 12, 1462–1468, doi: 10.1190/tle31121462.1.

Justinic, A. H., B. Stump, C. Hayward, and C. Frohlich (2013). Analysis of the Cleburne, Texas, earthquake sequence from June 2009 to June 2010, *Bull. Seismol. Soc. Am.* **103,** no. 6, 3083–3093, doi: 10.1785/0120120336.

Keller, G. R., and R. D. Hatcher Jr. (1999). Some comparisons of the structure and evolution of the southern Appalachian–Ouachita orogeny and portions of the Trans-European suture zone region, *Tectonophysics* **314,** nos. 1/3, 43–68, doi: 10.1016/S0040-1951(99)00236-X.

Keranen, K. M., and M. Weingarten (2018). Induced seismicity, *Annu. Rev. Earth Planet. Sci.* **46,** 149–174, doi: 10.1146/annurev-earth-082517-010054.

Keranen, K. M., M. Weingarten, G. A. Abers, B. A. Bekins, and S. Ge (2014). Sharp increase in central Oklahoma seismicity since 2008 induced by massive wastewater injection, *Science* **345,** no. 6195, 448–451, doi: 10.1126/science.1255802.

Lund Snee, J. E., and M. D. Zoback (2016). State of stress in Texas: Implications for induced seismicity, *Geophys. Res. Lett.* **43,** no. 19, doi: 10.1002/2016GL070974.

Magnani, M. B., M. L. Blanpied, H. R. DeShon, and M. J. Hornbach (2017). Discriminating between natural vs. induced seismicity from long-term deformation history of intraplate faults, *Sci. Adv.* **3,** no. 11, doi: 10.1126/sciadv.1701593.

Nuttli, O. W. (1973). Seismic wave attenuation and magnitude relations for eastern North America, *J. Geophys. Res.* **78,** 876–885, doi: 10.1029/JB078i005p00876.

Ogwari, P. O., H. R. DeShon, and M. J. Hornbach (2018). The Dallas-Fort Worth airport earthquake sequence: Seismicity beyond injection period, *J. Geophys. Res.* **123,** doi: 10.1002/2017JB015003.

Patton, J. M., M. R. Guy, H. M. Benz, R. P. Buland, B. K. Erickson, and D. S. Kragness (2016). Hydra—The National Earthquake Information Center's 24/7 seismic monitoring, analysis, catalog production, quality analysis, and special studies tool suite, *U.S. Geol. Surv. Open-File Rept. 2016-1128*, 28 pp., doi: 10.3133/ofr20161128.

Pavlis, G. L., F. Vernon, D. Harvey, and D. Quinlan (2004). The generalized earthquake-location (GENLOC) package: An earthquake-location library, *Comput. Geosci.* **30,** nos. 9/10, 1079–1091, doi: 10.1016/j.cageo.2004.06.010.

Pollastro, R. M., D. M. Jarvie, R. J. Hill, and C. W. Adams (2007). Geologic framework of the Mississippian Barnett Shale, Barnett-Paleozoic total petroleum system, Bend Arch-Fort Worth basin, Texas, *AAPG Bulletin* **91,** no. 4, 405–436, doi: 10.1306/10300606008.

Quinones, L. A., H. R. DeShon, M. B. Magnani, and C. Frohlich (2018). Stress orientations in the Fort Worth basin, Texas, determined from earthquake focal mechanisms, *Bull. Seismol. Soc. Am.* **108,** no. 3A, 1124–1132, doi: 10.1785/0120170337.

Reiter, D., M. Leidig, S. H. Yoo, and K. Mayeda (2012). Source characteristics of seismicity associated with underground wastewater disposal: A case study from the 2008 Dallas-Fort Worth earthquake sequence, *The Leading Edge* **31,** no. 12, 1454–1460, doi: 10.1190/tle31121454.1.

Richter, C. F. (1935). An instrumental earthquake magnitude scale, *Bull. Seismol. Soc. Am.* **25,** no. 1, 1–32.

Rubinstein, J. L., W. L. Ellsworth, and S. L. Dougherty (2018). The 2013-2016 induced earthquakes in Harper and Sumner Counties, southern Kansas, *Bull. Seismol. Soc. Am.* **108,** no. 2, 674–689, doi: 10.1785/0120170209.

Rubinstein, J. L., W. L. Ellsworth, A. McGarr, and H. M. Benz (2014). The 2001-present induced earthquake sequence in the Raton basin of northern New Mexico and southern Colorado, *Bull. Seismol. Soc. Am.* **104,** no. 5, 2162–2181, doi: 10.1785/0120140009.

Savvaidis, A., B. Young, D.-G. Huang, and A. Lomax (2019). TexNet: A Statewide Seismological Network in Texas, *Seismol. Res. Lett.* doi: 10.1785/0220180350.

Scales, M., H. R. DeShon, M. B. Magnani, J. I. Walter, L. Quinones, T. L. Pratt, and M. J. Hornbach (2017). A decade of induced slip on the causative fault of the 2015 Mw4.0 Venus earthquake, northeast Johnson County, Texas, *J. Geophys. Res.* **122,** 7879–7894, doi: 10.1002/2017JB014460.

Segall, P., and S. Lu (2015). Injection-induced seismicity: Poroelastic and earthquake nucleation effects, *J. Geophys. Res.* **120,** no. 7, 5082–5103, doi: 10.1002/2015JB012060.

Smye, K. M., C. R. Lemons, R. Eastwood, G. McDaid, and P. H. Hennings (2019). Stratigraphic Architecture and Petrophysical Characterization of Formations for Deep Disposal in the Fort Worth basin, TX, *Interpretation* doi: 10.1190/INT2018-0195.1.

Sufri, O., P. Ogwari, L. Quinones, and H.R. DeShon (2018). High resolution seismogenic fault imaging using double difference relocation in Azle-Reno, TX, *2018 Fall Meeting, American Geophysical Union*, Washington, D.C, 10–14 December.

Walter, J. I., P. J. Dotray, C. Frohlich, and J. Gale (2016). Earthquakes in northwest Louisiana and the Texas–Louisiana border possibly induced by energy resource activities within the Haynesville Shale Play, *Seismol. Res. Lett.* **87,** no. 2A, doi: 10.1785/0220150193.

Weingarten, M., S. Ge, J. W. Godt, B. A. Bekins, and J. L. Rubinstein (2015). High-rate injection is associated with the increase in US mid-continent seismicity, *Science* **348,** no. 6241, 1336–1340, doi: 10.1126/science.aab1345.

Wiemer, S., and M. Wyss (2000). Minimum magnitude of completeness in earthquake catalogs: Examples from Alaska, the western United States, and Japan, *Bull. Seismol. Soc. Am.* **90,** no. 4, 859–869, doi: 10.1785/0119990114.

Woessner, J., and S. Wiemer (2005). Assessing the quality of earthquake catalogues: Estimating the magnitude of completeness and its uncertainty, *Bull. Seismol. Soc. Am.* **95,** no. 2, 684–698, doi: 10.1785/0120040007.

Zhai, G., and M. Shirzaei (2018). Fluid injection and time-dependent seismic hazard in the Barnett Shale, Texas, *Geophys. Res. Lett.* **45,** no. 10, 4743–4753, doi: 10.1029/2018GL077696.

Louis Quinones
Heather R. DeShon
SeongJu Jeong
Oner Sufri
Kevin B. Kwong
Huffington Department of Earth Sciences
Southern Methodist University
P.O. Box 750395
Dallas, Texas 75275-0395 U.S.A.
hdeshon@smu.edu

Paul Ogwari
Oklahoma Geological Survey
100 E. Boyd Street, Suite N131
Norman, Oklahoma 73019 U.S.A.

Monique M. Holt
Department of Geology and Geophysics
115 S 1460 E, Room 383
Salt Lake City, Utah 84112-0102 U.S.A.

Manuscript received 2 March 2019;
Published Online 11 June 2019